

## COMOVING SPACE DENSITY OF X-RAY-SELECTED ACTIVE GALACTIC NUCLEI

J. D. SILVERMAN,<sup>1,2</sup> P. J. GREEN,<sup>1</sup> W. A. BARKHOUSE,<sup>1</sup> R. A. CAMERON,<sup>1</sup> C. FOLTZ,<sup>3</sup> B. T. JANNUZI,<sup>4</sup> D.-W. KIM,<sup>1</sup>  
M. KIM,<sup>1</sup> A. MOSSMAN,<sup>1</sup> H. TANANBAUM,<sup>1</sup> B. J. WILKES,<sup>1</sup> M. G. SMITH,<sup>5</sup> R. C. SMITH,<sup>5</sup> AND P. S. SMITH<sup>6</sup>

Received 2004 June 14; accepted 2005 February 1

### ABSTRACT

For measurement of the active galactic nucleus (AGN) luminosity function and its evolution, X-ray selection samples all types of AGNs and provides reduced obscuration bias in comparison with UV excess or optical surveys. The apparent decline in optically selected quasars above  $z \sim 3$  may be strongly affected by such a bias. The *Chandra* Multiwavelength Project (CHAMP) is characterizing serendipitously detected X-ray sources in a large number of fields with archival *Chandra* imaging. We present a preliminary measure of the comoving space density using a sample of 311 AGNs found in 23 CHAMP fields ( $\sim 1.8 \text{ deg}^2$ ) supplemented with 57 X-ray-bright AGNs from the Chandra Deep Field-North and Chandra Deep Field-South. Within our X-ray flux ( $f_{0.3-8.0 \text{ keV}} > 4 \times 10^{-15} \text{ ergs cm}^{-2} \text{ s}^{-1}$ ) and optical magnitude ( $r' < 22.5$ ) limits, our sample includes 14 broad emission-line AGNs at  $z > 3$ . Using this X-ray-selected sample, we detect a turnover in the comoving space density of luminous type 1 AGNs ( $\log L_X > 44.5 \text{ ergs s}^{-1}$ , measured in the 0.3–8.0 keV band and corrected for Galactic absorption) at  $z > 2.5$ . Our X-ray sample is the first to show a behavior similar to the well-established evolution of the optical quasar luminosity function. A larger sample of high-redshift AGNs and with a greater fraction of identified sources, either spectroscopic or photometric, at faint optical magnitudes ( $r' > 22.5$ ) are required to remove the remaining uncertainty in our measure of the X-ray luminosity function, particularly given the possibility that AGNs might be more easily obscured optically at high redshift. We confirm that for  $z < 1$ , lower luminosity AGNs ( $\log L_X < 44.5$ ) are more prevalent by more than an order of magnitude than those with high luminosity. We have combined the *Chandra* sample with AGNs from the *ROSAT* surveys to present a measure of the space density of luminous type 1 AGNs in the soft X-ray band (0.5–2.0 keV) that confirms the broadband turnover described above.

*Subject headings:* galaxies: active — quasars: general — surveys — X-rays: galaxies

### 1. INTRODUCTION

Optical surveys have measured the evolution of QSOs out to  $z \sim 6$  (Fan et al. 2004). The most dramatic feature found is the rise and fall of the comoving space density with peak activity at  $z \sim 2.5$ . A systematic decrease in luminosity from  $z \sim 2$  to the present is evident with very few intrinsically bright QSOs in the local universe (e.g., Croom et al. 2004). This fading of the QSO population is attributed to a decreased fuel supply and/or fueling rate (e.g., Cavaliere & Vittorini 2000; Kauffmann & Haehnelt 2000). The dropoff in the space density at  $z > 3$  (e.g., Warren et al. 1994; Schmidt et al. 1995; Fan et al. 2001; Wolf et al. 2003) could represent the growth phase of supermassive black holes (SMBHs), possibly under a veil of obscuration (Fabian 1999).

It has become clear over the past decade that X-ray selection of active galactic nuclei (AGNs) offers many benefits over detection methods in other wavebands. X-rays can penetrate large absorbing columns of gas that can effectively hide an accreting black hole in the optical. The existence of a significant, missed population of obscured AGNs is required to explain the spectral shape of the cosmic X-ray background (CXRB; e.g., Gilli et al. 2001). The current generation of X-ray observatories (*Chandra*, *XMM-Newton*) are probing the faint source population responsible for

the bulk of the CXRB (e.g., Alexander et al. 2003; Rosati et al. 2002; Hasinger et al. 2001).

X-ray surveys with *Chandra*, *XMM-Newton*, and *ASCA* are refining our knowledge of the AGN X-ray luminosity function. The peak, in the comoving space density of low-luminosity ( $L_{2.0-8.0 \text{ keV}} < 10^{44} \text{ ergs s}^{-1}$ ) AGNs found in hard (2–10 keV) X-ray surveys (Barger et al. 2003; Cowie et al. 2003; Fiore et al. 2003; Steffan et al. 2003; Ueda et al. 2003), occurs at  $z \sim 1$ . This contrasts starkly with the behavior of the luminous ( $L_{2.0-8.0 \text{ keV}} > 10^{44} \text{ ergs s}^{-1}$ ) QSOs, which are most prevalent at  $z \sim 2.5$ . Using a highly complete sample of 941 AGNs selected in the soft band, Hasinger et al. (2005) show the same luminosity dependence and extend the space density measurement of low-luminosity AGNs ( $L_X < 10^{44} \text{ ergs s}^{-1}$ ) out to  $z \sim 3$ . These latest results clearly require a luminosity-dependent density evolution model (Miyaji et al. 2000) in contrast to a “pure” luminosity evolution model, descriptive of optically selected QSOs (Croom et al. 2004). With these results, semianalytic models (Menci et al. 2004) posit that the more luminous QSOs illuminate early epochs when most of the massive galaxies are forming ( $z > 2$ ), thereby inducing high accretion rates, whereas lower luminosity AGNs dominate at a later period ( $z < 2$ ) when most of the galaxies have fully assembled.

X-ray-selected QSOs from *ROSAT* have hinted at a constant space density in the range  $1.5 < z < 4.5$  (Miyaji et al. 2000) for the most luminous AGNs ( $\log L_{0.3-8.0 \text{ keV}} > 44.5$ ). The lack of a decline in the space density at  $z > 3$ , in contrast to the behavior seen in optical surveys, could be evidence for obscuration at early epochs. We can test this model (Fabian 1999) by measuring the luminosity function and comoving space density of X-ray-selected AGNs over a wide area to compile a significant sample at  $z > 3$ . Unfortunately, the *ROSAT* sample includes only seven QSOs at these high redshifts. Of these, only five QSOs have

<sup>1</sup> Harvard-Smithsonian Center for Astrophysics, 60 Garden Street, Cambridge, MA 02138; jsilverman@mpe.mpg.de.

<sup>2</sup> Astronomy Department, University of Virginia, P.O. Box 3818, Charlottesville, VA 22903-0818.

<sup>3</sup> National Science Foundation, 4201 Wilson Boulevard, Arlington, VA 22230.

<sup>4</sup> National Optical Astronomy Observatory, P.O. Box 26732, Tucson, AZ 85726-6732.

<sup>5</sup> Cerro Tololo Inter-American Observatory, National Optical Astronomical Observatory, Casilla 603, La Serena, Chile.

<sup>6</sup> Steward Observatory, University of Arizona, Tucson, AZ 85721.

luminosities high enough to be detected over a broad range of redshift ( $0 < z < 5$ ) and therefore included in the measurement of the comoving space density (Miyaji et al. 2000). While the *Chandra* and *XMM-Newton* Deep Field observations have great scientific merit, their narrow area provides only four high-luminosity ( $\log L_{0.3-8.0 \text{ keV}} > 44.5$ ) AGNs at  $z > 3$ . Recent measurement of the hard X-ray luminosity function (Barger et al. 2003; Fiore et al. 2003; Steffan et al. 2003; Ueda et al. 2003) have limited numbers of AGNs at these high redshifts. A wider area survey is needed to compile a significant sample of highly luminous QSOs with redshifts greater than 3.

We present a preliminary measure of the comoving space density of X-ray-selected AGNs out to  $z \sim 4$  from the *Chandra* Multiwavelength Project (CHAMP). We supplement the CHAMP sample with AGNs of comparable X-ray and optical fluxes from the *Chandra* Deep Field-North (CDF-N) and *Chandra* Deep Field-South (CDF-S) to boost our spectroscopic completeness at faint optical magnitudes and include one additional  $z > 3$  QSO. We merge the subsample of these AGNs detected in the soft (0.5–2.0 keV) band with those from *ROSAT* to directly compare our results with those of Miyaji et al. (2000, 2001). A full presentation of the CHAMP X-ray luminosity function is forthcoming (J. Silverman et al. 2005, in preparation). We assume  $H_0 = 70 \text{ km s}^{-1} \text{ Mpc}^{-1}$ ,  $\Omega_\Lambda = 0.7$ , and  $\Omega_M = 0.3$  with the exception of those parameters used in § 6.2.

## 2. CHANDRA MULTIWAVELENGTH PROJECT

The CHAMP (Kim et al. 2004a; Green et al. 2004) is carrying out an extragalactic X-ray survey encompassing  $10 \text{ deg}^2$  using serendipitous detections in archival *Chandra* fields. *Chandra*'s small point-spread function ( $\sim 1''$  resolution on-axis) and low background allow sources to be detected to fainter flux levels ( $\sim 10^{-15} \text{ ergs cm}^{-2} \text{ s}^{-1}$ ) than any X-ray observatory past or present, thus enabling the detection of high-redshift ( $z \sim 5$ ) AGNs (Treister et al. 2004; Barger et al. 2003; Castander et al. 2003; Silverman et al. 2002). For this study, we use the full *Chandra* energy range (0.3–8.0 keV) to detect the absorbed sources missed by previous optical, UV, or soft X-ray surveys, and we take advantage of the high collecting area at soft energies to detect the faint, high-redshift AGNs. At  $z > 3$ , our survey is sensitive to AGNs with absorbing columns up to  $\sim 10^{23} \text{ cm}^{-2}$  owing to the favorable  $k$ -correction. With a sample of AGNs selected from a large number of noncontiguous *Chandra* fields that reach similar depths ( $\sim 10^{-15} \text{ ergs cm}^{-2} \text{ s}^{-1}$ ), we effectively smooth out any effects from large-scale structures such as those evident in the CDF-S (Gilli et al. 2003).

We have chosen 23 *Chandra* fields ( $1.8 \text{ deg}^2$ ) for which we have acquired extensive follow-up optical imaging and spectroscopy. The deepest observations have exposure times that are sensitive to sources with  $f_{0.3-8.0 \text{ keV}} > 8 \times 10^{-16} \text{ ergs cm}^{-2} \text{ s}^{-1}$ . A full description of the CHAMP image reduction and analysis pipeline XPIPE can be found in Kim et al. (2004b). With our 4 m MOSAIC optical imaging, we are able to identify counterparts to the *Chandra* sources down to  $r' \sim 25$  (Green et al. 2004). We acquire optical imaging in three ( $g'$ ,  $r'$ , and  $i'$ ) Sloan Digital Sky Survey (SDSS) filters (Fukugita et al. 1996). Optical colors provide preliminary source classification and crude photometric redshifts. These diagnostics are required to characterize the optically faint X-ray sources that cannot be identified with spectroscopy and, in particular, their influence on the X-ray luminosity function. The use of the SDSS photometric system allows more direct comparison between the CHAMP and the SDSS AGN surveys (Silverman et al. 2004). Optical spectroscopic follow-up currently focuses on identifying counterparts with  $r' < 22.5$  for which

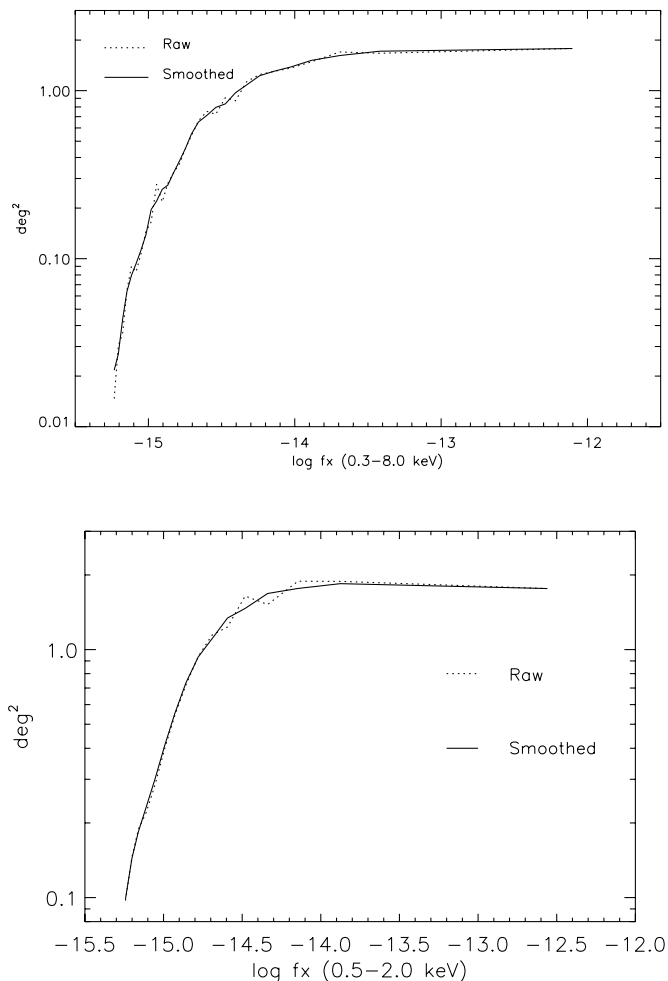


FIG. 1.—Area coverage as a function of broad (0.3–8.0 keV; top) and soft (0.5–2.0 keV; bottom) band X-ray flux for 23 CHAMP fields. A smoothed curve is generated since small-scale variations or sharp features are a result of the limited number of simulated sources and are not real.

spectra can be acquired on a 4–6 m (i.e., MMT, Magellan, WIYN, CTIO Blanco) class telescope. To date, we have spectroscopically classified a sample of 358 AGNs detected in the broad band (0.3–8.0 keV) in these 23 CHAMP fields.

## 3. X-RAY SENSITIVITY AND AREA COVERAGE

There are complications with measuring the X-ray luminosity function that must be put into context. The difficulty in focusing X-rays results in a point-source function (PSF) and flux sensitivity that varies across the field of view. The PSF degrades as a function of off-axis angle, decreasing the flux sensitivity. In terms of measuring the luminosity function, it is not a trivial task to determine the incompleteness at the faintest X-ray fluxes and the actual sky area over which a source of a specific flux would be detected. In addition, the exposure times of these *Chandra* fields range from 17 to 114 ks, generating a wide range of limiting fluxes even on-axis.

To characterize the sensitivity, completeness, and sky area coverage as a function of X-ray flux, a series of simulations were performed. The full details will be presented in an upcoming CHAMP X-ray analysis paper (M. Kim et al. 2005, in preparation). The simulations consists of three parts: (1) generating artificial X-ray sources with MARX (MARX Technical Manual<sup>7</sup>)

<sup>7</sup> See <http://space.mit.edu/CXC/MARX>.

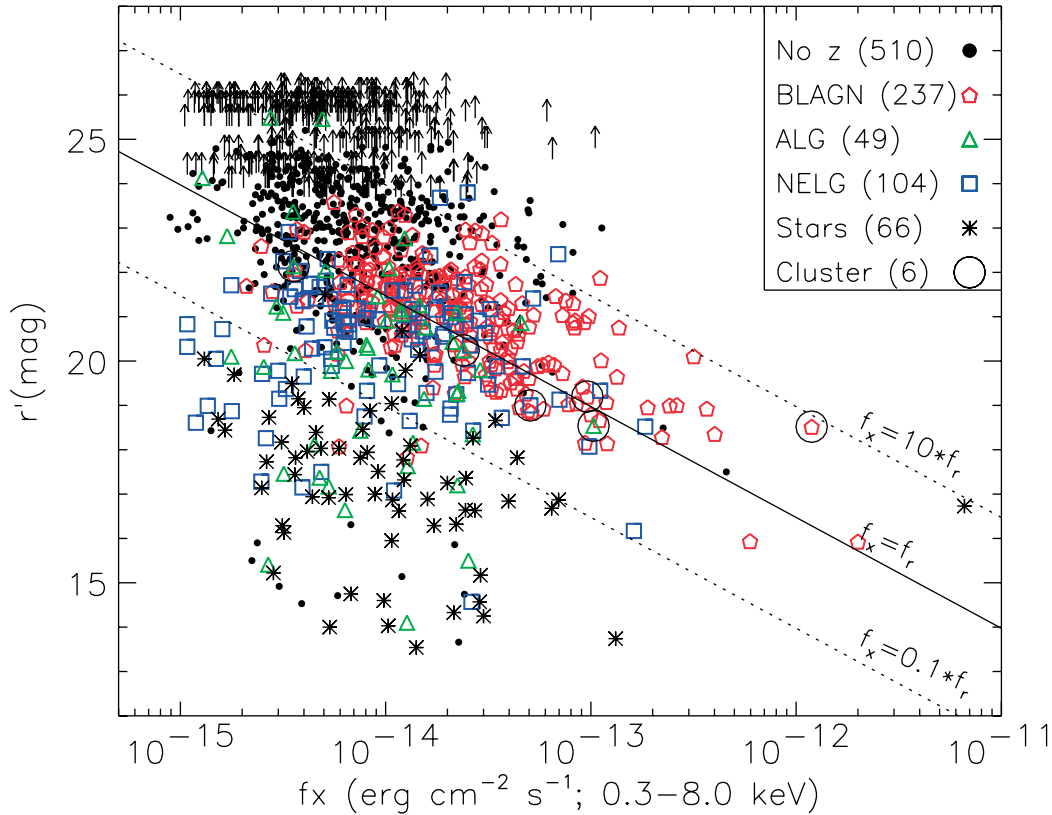


FIG. 2.—Optical magnitude ( $r'$ ) vs. X-ray flux (0.3–8 keV) of X-ray sources found in 23 CHAMP fields. Optical spectroscopic classifications are indicated with the sample size. X-ray sources with no optical counterparts are shown by an arrow placed at the magnitude for a  $5\sigma$  detection from our optical imaging.

and adding them to real X-ray images, (2) detecting these artificial sources using *wavdetect* and extracting source properties with XPIPE identically as performed for actual sources, and (3) estimating the sky area coverage by comparing the input and detected source properties as a function of flux. The simulations are restricted to specific CCDs for ACIS-I (I0, I1, I2, and I3) and ACIS-S (I2, I3, S2, and S3). These CCDs are closest to the aim point for each observation. Sources far off-axis ( $\Theta > 12'$ ) are excluded since the flux sensitivity is low and the PSF is degraded. These simulations allow determination of corrections for the source detection incompleteness at faint flux levels quantified in the first CHAMP X-ray analysis paper (Kim et al. 2004b). In Figure 1 we show the sky coverage determined from the simulations using the broad (0.3–8.0 keV) and soft (0.5–2.0 keV) band source detections for 23 CHAMP fields. We are surveying a sky area of  $1.8 \text{ deg}^2$  for the brightest sources. The sky area falls below  $0.1 \text{ deg}^2$  at the faintest flux levels.

#### 4. AGN SELECTION

In these CHAMP fields, we find a diversity of objects (AGNs, clusters, galaxies, and stars), although 85% of them are attributed to an AGN (Green et al. 2004; Silverman et al. 2004). We show the optical magnitude ( $r'$ ) as a function of 0.3–8.0 keV X-ray flux for the sources detected in 23 CHAMP fields (Fig. 2). We only include sources with greater than 9.5 net counts. Although sources with counts as low as 2 may be significant detections as a result of *Chandra*'s low background, we use a higher count limit to ensure that we have well-measured X-ray fluxes within our sample. In Figure 2 we label sources as classified from our optical spectroscopy. Extragalactic objects with strong emis-

sion lines ( $W_\lambda > 5 \text{ \AA}$ ) are labeled as either broad-line AGNs (BLAGNs;  $\text{FWHM} > 1000 \text{ km s}^{-1}$ ) or narrow emission-line galaxies (NELGs;  $\text{FWHM} < 1000 \text{ km s}^{-1}$ ). The BLAGNs are equivalent to type 1 AGNs. We loosely refer to the NELGs with  $L_X > 10^{42} \text{ ergs s}^{-1}$  as type 2 AGNs, since optical spectra may not cover all the emission lines needed to confirm photoionization from a nonthermal source. Extragalactic counterparts with weak emission-line ( $W_\lambda < 5 \text{ \AA}$ ) or pure absorption-line spectra are classified as absorption-line galaxies (ALGs). In addition, a handful of stars are identified at faint X-ray fluxes. Six clusters have been found based primarily on their extended X-ray emission.

We calculate the rest-frame (0.3–8.0 keV;  $\text{ergs s}^{-1}$ ) X-ray luminosity for each extragalactic source, after correction for Galactic absorption. The conversion from X-ray count rate to flux units ( $\text{ergs cm}^{-2} \text{ s}^{-1}$ ) is determined from simulated detections on each CCD of a source with a power-law spectrum<sup>8</sup> [ $f_E \propto E^{-(\Gamma-1)}$ ;  $\Gamma = 1.7$ ] and galactic absorption (Dickey & Lockman 1990). The observed luminosity is converted to the rest frame assuming a power-law spectrum with the photon index ( $\Gamma$ ) set to the average value for that object type (BLAGN, NELG, ALG) on the basis of our X-ray spectral fit results (T. L. Aldcroft et al. 2005, in preparation). We find that the BLAGNs have a mean spectral index ( $\langle \Gamma \rangle$ ) of 1.9, while the NELGs have  $\langle \Gamma \rangle = 0.9$  and ALGs have  $\langle \Gamma \rangle = 1.5$ . We do not apply a correction for intrinsic absorption due to the uncertainty in the absorbing columns for most of these AGNs as a result of their low X-ray counts.

<sup>8</sup> The CHAMP XPIPE (Kim et al. 2004b) provides energy conversion factors for two models with  $\Gamma = 1.7$  and  $\Gamma = 1.4$ . We chose the former since the photon index more closely resembles the majority of the X-ray source detections with spectroscopic identification.

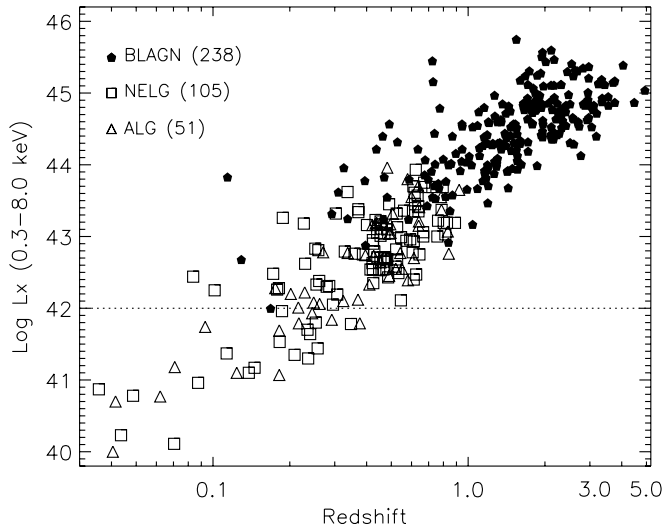


Fig. 3.—X-ray luminosity vs. redshift of 394 extragalactic objects found in 23 CHAMP fields (with the exception of six clusters). The dashed line marks the minimum luminosity required for the AGN sample. Optical spectroscopic classifications are shown as either BLAGNs, NELGs, or ALGs.

To construct a pure AGN sample, we require the derived (rest frame 0.3–8.0 keV) luminosity to exceed  $10^{42}$  ergs  $s^{-1}$ , thereby excluding any sources that contain a significant stellar or hot interstellar medium component. As shown in Figure 3, we see that 92% of the extragalactic sources in the CHAMP not associated with an extended X-ray-emitting cluster satisfy this criterion. We currently have not identified any NELGs or ALGs above a redshift of 1 in the CHAMP. Our optical spectroscopic limit ( $r' \sim 22$ ) precludes classification of objects with heavy optical extinction beyond this redshift, since a  $\sim 5L_*$  elliptical host galaxy has  $r' \sim 23$  at  $z \sim 1$ . We detect many optical type 2 AGNs with  $L_X < 10^{44}$  ergs  $s^{-1}$  but no luminous ( $L_X > 10^{44}$  ergs  $s^{-1}$ ) optical type 2 QSOs. We do find 6% of the BLAGNs to be X-ray-absorbed with a substantial fraction having reddened optical colors that may prevent them from being selected in optical surveys (Silverman et al. 2004). These red BLAGNs may be similar to those found by the Two Micron All Sky Survey (Francis et al. 2004) that tend to have significant X-ray-absorbing columns of gas (Wilkes et al. 2002). Deep optical follow-up of a broadband X-ray-selected sample will help determine the fraction of such red quasars to the space density of X-ray-luminous AGNs.

## 5. SURVEY COMPLETENESS

We have supplemented our CHAMP sample with X-ray sources from the CDF-N (Brandt et al. 2001; Barger et al. 2002) and CDF-S (Giacconi et al. 2002; Szokoly et al. 2004) with X-ray fluxes above our chosen limit (see below;  $f_{0.3-8.0 \text{ keV}} > 4 \times 10^{-15}$  ergs  $cm^{-2} s^{-1}$ ). These samples allow us to boost the number of spectroscopically identified sources at faint optical magnitudes ( $r' > 21$ ) and include any additional  $z > 3$  AGNs. These are currently the only surveys with published optical spectroscopic identifications at moderate completeness levels for sources with flux levels comparable to the CHAMP. In Figure 4 (top), we plot the flux distribution of X-ray sources found in these 25 *Chandra* fields. The CDF-N and CDF-S clearly contribute most of the faint sources ( $\log f_X < -15$ ). In Figure 4 (bottom), we show the optical magnitude distribution of counterparts to sources with X-ray fluxes above our chosen limit and those with optical spectroscopic identifications. Optical magnitudes for the CDF-N and CDF-S sources were converted from the Johnson

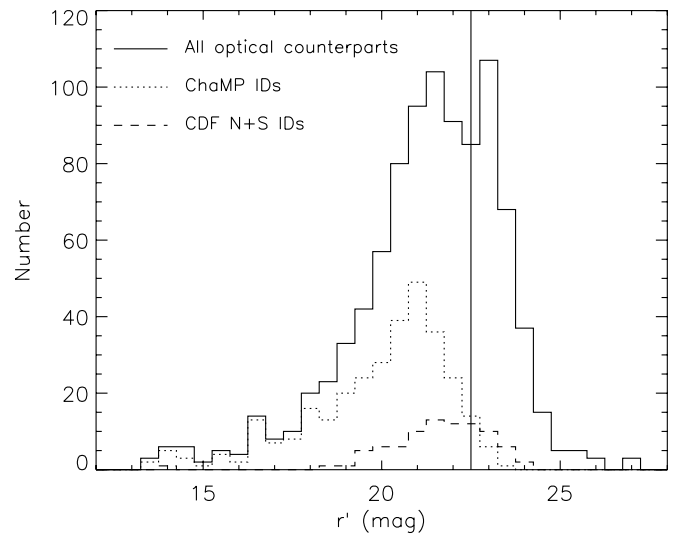
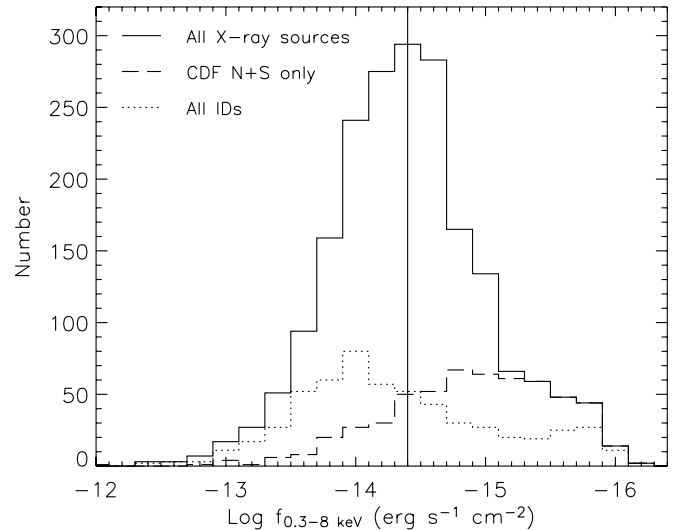


Fig. 4.—*Top*: X-ray (0.3–8.0 keV) flux distribution of 1989 sources in the CHAMP and CDF-N and CDF-S surveys (solid histogram). Those sources from only the CDF-N and CDF-S are shown as the long dashed line. Those with optical spectroscopic identifications are shown as the short dashed line. The vertical line marks the X-ray flux limit of  $f_{0.3-8.0 \text{ keV}} > 4 \times 10^{-15}$  ergs  $cm^{-2} s^{-1}$ . *Bottom*: Optical magnitude ( $r'$ ) distribution of counterparts to X-ray sources with fluxes above our limit. Counterparts with spectroscopic identification are shown with a short (CHAMP) or long (CDF-N and CDF-S) dashed line. The vertical line marks our chosen optical magnitude limit.

( $B$ ,  $R$ ) to the SDSS photometric system using the transformation in Fukugita et al. (1996). By including these two deep *Chandra* fields, our area coverage is larger than that shown in Figure 1. We add a fixed area of  $0.22 \text{ deg}^2$ , since the area coverage in these two fields does not change above this bright flux limit by more than 3%.

To evaluate the status of our optical follow-up and determine effective survey limits, we measure the fraction of X-ray sources identified with optical spectroscopic observations as a function of X-ray flux and optical magnitude. Since the X-ray sources do not fully sample the  $f_X$ - $r'$  plane (Fig. 2), we have implemented an adaptive binning scheme identical to that of Sanders & Fabian (2001) to generate a completeness map as a function of X-ray and optical flux for the combined sample (CHAMP + CDF-N + CDF-S). We create an array with  $64 \times 64$  elements covering the  $f_X$ - $r'$  plane (Fig. 2). The identified fraction  $f_{ID}$  is measured at

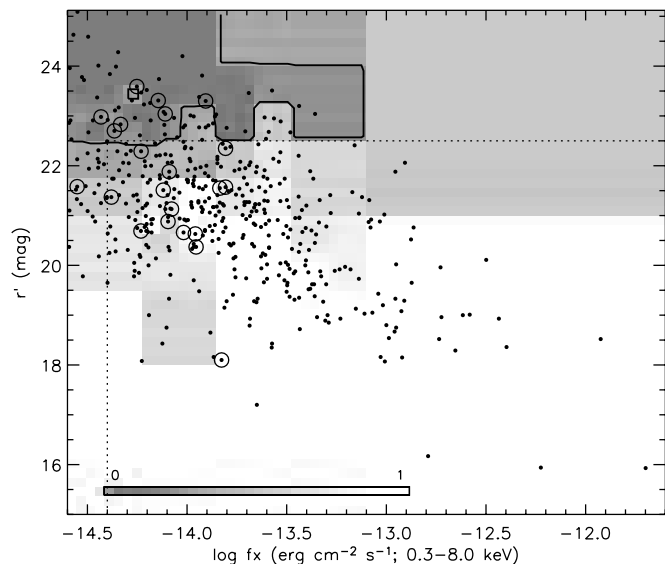


FIG. 5.—Adaptively binned spectroscopic completeness map. The shading scale ranges from zero (*lightest*) to 100% (*darkest*) spectroscopically classified. Only spectroscopically identified AGNs are shown with a black dot, and those at  $z > 3$  with circled dots. Dashed lines show our chosen flux limits. A solid contour line has been overplotted to mark the 30% completeness level.

each element as the number of identified objects divided by the number of X-ray sources. If 10 or more X-ray sources are in a single element, then we assign  $f_{\text{ID}}$  as the completeness level. We then increase the bin size by a factor of 2. If the binned element has 10 or more objects, the individual elements not previously assigned an identified fraction are set to this value. This procedure is iterated until the final binned element equals the size of the full array. In Figure 5, we plot the final array (i.e., completeness map) as a gray-scale image.

On the basis of Figure 5, we set the flux limits of our AGN sample. We choose a single X-ray flux limit at  $f_{0.3-8.0 \text{ keV}} > 4 \times 10^{-15} \text{ ergs cm}^{-2} \text{ s}^{-1}$  that is brighter than the faintest X-ray detections in the CHAMP. This limit ensures that we minimize the bias toward optically bright AGNs at the faintest X-ray flux limits. In order to limit our completeness correction to  $< 3.3$ , we set an optical magnitude limit at a level at which at least 30% of the sources are identified; this leads to a magnitude limit of 22.5. With the remaining sample, the incompleteness level is used to correct the measurement of the space density (§ 6).

In Figure 5, we plot the location of AGNs, including those from the CDFs in the  $f_x$ - $r'$  plane. Since a significant number of AGNs fall in regions of low completeness at faint fluxes, we must exclude eight of the 22 AGNs with  $z > 3$  and  $\log f_x > -14.6$  (*circled points*). In particular, the highest redshift AGN (CXOMP J213945.0–234655;  $z = 4.93$ ; Silverman et al. 2002) found by the CHAMP has been excluded not because of its X-ray flux ( $f_{0.3-8.0 \text{ keV}} = 4.32 \times 10^{-15} \text{ ergs cm}^{-2} \text{ s}^{-1}$ ) but rather because of its optical magnitude ( $r' = 22.7$ ), which falls below our limit. We do have a significant sample of 368 AGNs above our flux limits with 14 (13 from CHAMP) at  $z > 3$ , almost a factor of 3 larger than the high-redshift sample available from *ROSAT*. In Figure 6, we plot the  $L_x$ - $z$  distribution of the total sample of 368 AGNs selected in the 0.3–8.0 keV band.

## 6. COMOVING SPACE DENSITY

We implement the  $1/V_a$  method (Schmidt 1968) to generate an estimate to the comoving space density ( $n$  in units of  $\text{Mpc}^{-3}$ ; eq. [1]) in fixed redshift and luminosity intervals. For each

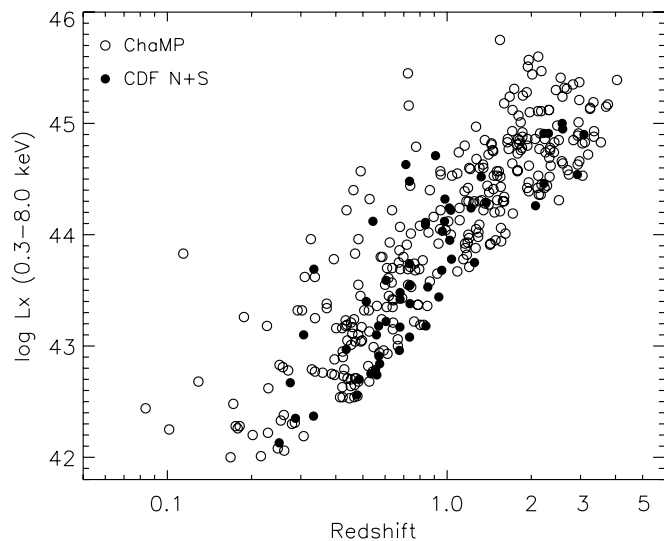


FIG. 6.—X-ray luminosity and redshift distribution of 368 AGNs (311 CHAMP + 57 CDF-N and CDF-S) with fluxes above our chosen limits.

$L$ - $z$  bin, equation (1) is summed over all AGNs ( $N$ ) from our sample (Fig. 6) that fall within this bin:

$$n = \sum_{i=1}^N \frac{1}{f_{\text{ID}} V_a(i)}. \quad (1)$$

As mentioned in § 3, our survey has noncontiguous sky coverage with varying flux limits. To account for this, we determine the accessible volume  $V_a$  (eq. [2]) over which an individual AGN  $i$  will be included in our sample, given the X-ray and optical flux limits

$$V_a = \int_{z_1}^{z_2} \frac{dV_c}{dz}. \quad (2)$$

We calculate the X-ray and optical limiting redshifts ( $z_{\text{lim}}^X, z_{\text{lim}}^O$ ) for each object. The integrand in equation (2) is summed from  $z_1$  to  $z_2$ , where  $z_2$  is the smaller of  $z_{\text{lim}}^X$  and  $z_{\text{lim}}^O$  if the AGN cannot be detected over the full redshift interval. The solid angle ( $\Omega$ ) is a function of X-ray flux as shown in Figure 1, plus an additional  $0.22 \text{ deg}^2$  contributed by the CDF observations. A correction factor ( $f_{\text{ID}}$ ), determined from the location of an individual AGN in the  $f_x$ - $r'$  plane (Fig. 5), compensates for the incompleteness in our spectroscopic identifications as detailed in the previous section. Each AGN contributes  $(f_{\text{ID}} V_a)^{-1}$  to the space density in a specific luminosity and redshift interval. We estimate  $1 \sigma$  errors on the basis of a Poisson distribution because of the small number of objects per bin. While there are known biases inherent in the  $1/V_a$  method (e.g., Miyaji et al. 2001; Page & Carrera 2000), the overall evolutionary trends can be discerned (e.g., Barger et al. 2003; Cowie et al. 2003; Fiore et al. 2003). A detailed X-ray luminosity function will be presented in a future publication (J. Silverman et al. 2005, in preparation) while implementing more sophisticated analysis techniques (e.g., maximum likelihood method).

### 6.1. Broad Band (0.3–8.0 keV)

We measure the comoving space density (eq. [1]) of AGNs detected in the broad band from 25 *Chandra* fields. In Figure 7, the number density is plotted in three luminosity bins ( $42.0 <$

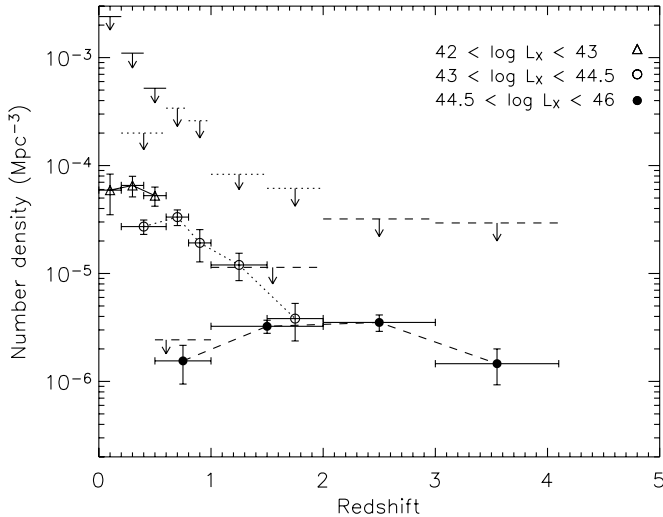


FIG. 7.—Comoving space density of AGNs selected in the broad (0.3–8.0 keV) band. Vertical bars represent estimates of the  $1\sigma$  error. Horizontal bars, centered on each data point, mark the redshift bin size. Horizontal bars with a downward arrow show the highly conservative upper limits that take into account the optically faint ( $r' > 22.5$ ), unidentified X-ray sources. The upper limits correspond to the data that have the same line type connecting the points.

$\log L_X < 43.0$ ,  $43.0 < \log L_X < 44.5$ , and  $44.5 < \log L_X < 46.0$ ;  $L$  is in units of  $\text{ergs s}^{-1}$ ) as a function of redshift. We must keep in mind that we are limited to the detection of obscured AGNs (type 2) at luminosities below  $10^{44}$   $\text{ergs s}^{-1}$  and redshifts below 1 owing to our optical spectroscopic limit, as shown in Figure 3. As a result, the highest luminosity range ( $44.5 < \log L_X < 46.0$ ) is restricted to type 1 AGNs only. To account for the optically faint ( $r' > 22.5$ ), spectroscopically unidentified X-ray sources, we remove the optical flux limit and implement the method of Cowie et al. (2003) and Barger et al. (2003) to measure upper limits to the space density. We have assigned all unidentified sources to each feasible  $L$ - $z$  bin with the redshift and luminosity set to the mean value. With this method, a specific source usually falls within multiple  $L$ - $z$  bins.

At  $z < 1$ , the low-luminosity ( $\log L_X < 44.5$ ) AGNs are more than an order of magnitude more numerous than those with high luminosity, thus confirming recent results (Cowie et al. 2003; Fiore et al. 2003; Ueda et al. 2003). This is evident even when considering the unidentified population, since the upper limit to the space density of luminous AGNs ( $\log L_X > 44.5$ ) at  $z < 1$  is fairly constrained. From Figure 3, we see that most of the sources contributing to the space density at  $z < 1$  are non-BLAGNs. These results agree with those reported by Steffan et al. (2003) that show type 2 AGNs as the dominant population at  $0.5 < z < 1$ . The peak values of the two lower luminosity curves [ $n \sim (3-7) \times 10^{-5} \text{ Mpc}^{-3}$ ] agree with those from the soft (0.5–2.0 keV) X-ray luminosity function (Hasinger et al. 2005).<sup>9</sup> We find the space density to be a factor of  $\sim 3$  less, for AGNs with  $43.0 < \log L_X < 44.5$  at  $z \sim 0.8$ , than the hard (2–10 keV) X-ray survey results of Ueda et al. (2003). These comparisons seem reasonable since our broadband (0.3–8.0 keV) selected sample will be affected by absorption, as is known to occur in samples selected in the soft band (0.5–2.0 keV).

For the luminous AGNs ( $\log L_X > 44.5$ ), we measure a rise and fall of the number density with a peak at  $z \sim 2.5$ . With 14 AGNs in the high-redshift bin ( $3 < z < 4.2$ ), we have evidence

for a drop in the density that is inconsistent (at  $3.4\sigma$ ) with the peak value found at  $2 < z < 3$ . This result is not strongly affected by our bright optical magnitude limit since most AGNs at  $z > 3$  do not all fall near the flux limit, as shown in Figure 5. However, given the large numbers of unidentified sources, the upper limits to the space density at  $z > 2$  (Fig. 7) show considerable uncertainty. A higher fraction of identified X-ray sources is required to determine if a decline is present with high significance. The peak in the space density appears to shift to lower redshift with decreasing luminosity as modeled by luminosity-dependent density evolution (Ueda et al. 2003; Miyaji et al. 2000), in contrast to pure luminosity evolution reported by the optical surveys of bright quasars (e.g., Croom et al. 2004).

## 6.2. Soft Band (0.5–2.0 keV): *Chandra*+*ROSAT*

With *Chandra*'s broad energy range, we can select an AGN sample in the soft band (0.5–2.0 keV) to directly compare with the *ROSAT* results. The CHAMP AGNs, supplemented by those in the CDFs, can be combined with the *ROSAT* sample (Miyaji et al. 2000) to measure the number density of AGNs in the soft band with significant numbers of type 1 AGNs up to  $z \sim 4$ . The *ROSAT* sample is a compilation of AGNs found in surveys spanning the pencil beam ( $0.3 \text{ deg}^2$ ), deep Lockman Hole (Lehmann et al. 2001) to the wide-area ( $2.0 \times 10^4 \text{ deg}^2$ ), shallow *ROSAT* Bright survey (Schwope et al. 2000). To directly compare our sample with the published results from the *ROSAT* and optical surveys such as the Two-Degree Field (2dF; Croom et al. 2004), SDSS (Fan et al. 2001), and COMBO-17 (Wolf et al. 2003), we use cosmological parameters  $\Omega_M = 1$ ,  $\Omega_\Lambda = 0$ , and  $H_0 = 50 \text{ km s}^{-1} \text{ Mpc}^{-1}$ . The luminosity is calculated in the observed frame (no  $k$ -correction) to compare with the *ROSAT* results (Miyaji et al. 2000). We have assembled a total of 1004 AGNs with  $L_{0.5-2.0 \text{ keV}} > 10^{42} \text{ ergs s}^{-1}$ ,  $f_X > 2 \times 10^{-15} \text{ ergs cm}^{-2} \text{ s}^{-1}$ , and  $r' < 22.5$  (Fig. 8). The CHAMP AGNs boost the numbers at high redshift and lower luminosity because of *Chandra*'s faint limiting flux. Following the analysis of Miyaji et al. (2000), we measure the comoving space density for luminous ( $\log L_{0.5-2.0 \text{ keV}} > 44.5$ ) AGNs to ensure that we are sensitive to these objects out to  $z \sim 4$ . This minimum luminosity ensures that our measurements are not highly biased by our X-ray flux limit.

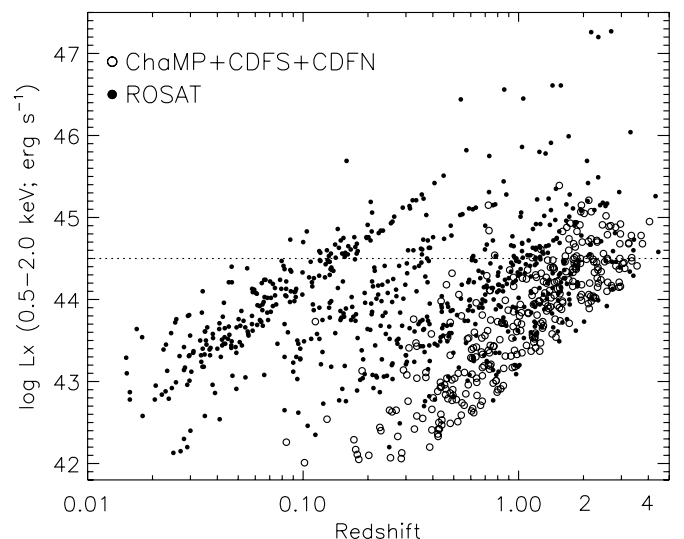


FIG. 8.—X-ray luminosity vs. redshift of 1004 AGNs selected in the soft (0.5–2.0 keV) band with *ROSAT* and *Chandra*. The horizontal line shows our threshold for measuring the space density of highly luminous AGNs.

<sup>9</sup> Also reproduced in Fig. 8a of a review article on deep extragalactic X-ray surveys by Brandt & Hasinger (2004).

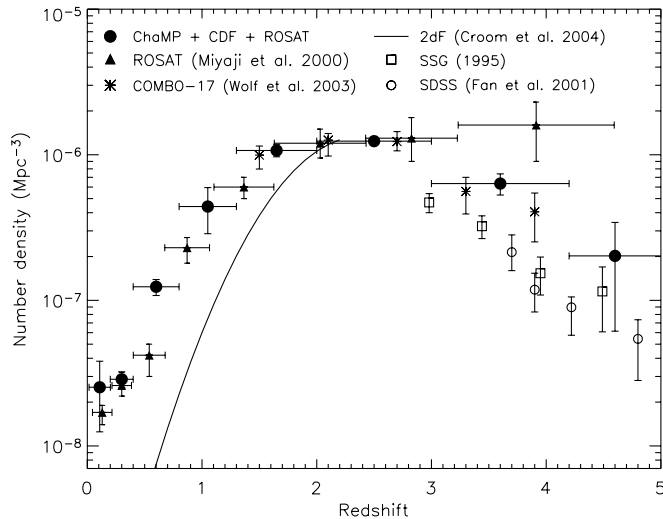


Fig. 9.—Comoving space density of 217 *Chandra* + *ROSAT* AGNs selected in the soft (0.5–2.0 keV) band with  $\log L_X > 44.5$  compared to the optical surveys. The optical space densities have been scaled to match the X-ray points at  $z = 2.5$  for ease of comparison.

In Figure 9, we plot the comoving space density of the 217 most X-ray-luminous AGNs. With these highly luminous AGNs, we can compare the space density to past *ROSAT* results and optical surveys out to high redshift ( $z < 5$ ). To easily compare the space density evolution from optical surveys, in Figure 9, we have renormalized their curves to match the CHAMP at  $z = 2.5$ . For all but the COMBO-17 survey, optical space densities ( $M_B < -26$ ) have been scaled up by a factor of 3.2. The COMBO-17 survey, which reaches much greater depths ( $R < 24$ ), was scaled down by a factor of 7.1. Some caution must be taken when comparing optical surveys with vastly different magnitude limits. For example, the AGNs in the 2dF survey evolve faster than those from X-ray-selected samples at  $z < 2$  (Fig. 9). The COMBO-17 survey, which probes similar absolute magnitudes ( $M_B < -22.2$ ) as the CHAMP, may show evolution rates comparable to the X-ray surveys over the redshift interval  $1.5 < z < 2.1$ .

The number density of our combined sample is similar to the *ROSAT* results with  $z < 3$ . Our larger  $z > 3$  sample (12 AGNs), while statistically consistent with the earlier results of Miyaji et al. 2000), has smaller errors and shows a decrease in the space density from  $2 < z < 3$  to  $3 < z < 4.2$ , significant at the  $4.6 \sigma$  level. Even with the addition of *ROSAT* AGNs, we have a slightly smaller sample at  $z > 3$  than in the broadband sample (§ 6.1) as a result of lower fluxes, luminosity, or counts in the soft band for the CHAMP AGNs. We find reasonable agreement with a slight excess between the relative drop in the space density of the X-ray and optical surveys at  $z > 2$ ; our data are consistent with a decline in the X-ray luminosity function similar to that observed in the optical.

## 7. CONCLUSION

We have measured the broadband (0.3–8.0 keV) comoving space density using a sample of 368 X-ray-emitting AGNs detected by *Chandra*. Our spectroscopic magnitude limit to date allows the inclusion of optically obscured AGNs to  $z \leq 1$  and unobscured AGNs out to  $z \sim 4$ .

Our primary results are as follows:

1. We confirm that low-luminosity AGNs ( $\log L_X < 44.5$ ) are more prevalent at  $z < 1$  than higher luminosity AGNs, as seen by Cowie et al. (2003), Fiore et al. (2003), and Ueda et al. (2003). Non-BLAGNs are the major contributor to the comoving space density at these low redshifts, as reported by Steffan et al. (2003).

2. The space density of type 1, highly luminous ( $\log L_X > 44.5$ ) X-ray-selected AGNs rises from the present epoch to a peak at  $z \sim 2.5$  and then declines at  $z > 3$ . This behavior is similar to that of optically selected surveys. This is the first X-ray-selected survey to detect a decline at high redshifts. The evolution is evident using a sample of 311 AGNs from the CHAMP selected in the broad (0.3–8.0 keV) *Chandra* band and 217 luminous QSOs selected in the soft band (0.5–2.0 keV) from *Chandra* and *ROSAT*.

Our results support a more rapid depletion of fuel for the high-luminosity AGNs from  $z \sim 2.5$  to the present epoch (Menci et al. 2004), perhaps because of their higher accretion rate. At  $z < 1$ , the lower luminosity AGNs evolve slowly, which may be attributable to a low accretion rate, compared to the more luminous AGNs. At  $z > 3$ , the decline in the space density of highly luminous AGNs represents the growth phase of SMBHs during a period of rapid galaxy assembly. The uncertainties in the X-ray luminosity function will improve with larger samples and a higher fraction of source classification, either through spectroscopic or photometric techniques. With the inclusion of obscured, highly luminous QSOs, X-ray surveys are well on the way to presenting a more comprehensive view of AGN evolution.

We are greatly indebted to NOAO and the SAO TACs for their support of this work. We thank the staffs at KPNO, CTIO, Las Campanas, W. M. Keck Observatory, FLWO, and MMT for assistance with optical observations. We thank John Huchra for his suggestions on dealing with complex selection effects. We also thank Takamitsu Miyaji and Guenther Hasinger for providing us with the *ROSAT* AGN catalog. We gratefully acknowledge support for this project under NASA CXC archival research grants AR3-4018X and AR4-5017X. T. L. A., R. A. C., P. J. G., D. W. K., A. E. M., H. T., and B. W. also acknowledge support through NASA contract NAS8-39073 (CXC).

## REFERENCES

- Alexander, D. M., et al. 2003, *AJ*, 126, 539  
 Barger, A. J., Cowie, L. L., Capak, P., Alexander, D. M., Bauer, F. E., Brandt, W. N., Garmire, G. P., & Hornschemeier, A. E. 2003, *ApJ*, 584, L61  
 Barger, A. J., et al. 2002, *AJ*, 124, 1839  
 Brandt, W. N., & Hasinger, G. 2005, preprint (astro-ph/0501058)  
 Brandt, W. N., et al. 2001, *AJ*, 122, 2810  
 Castander, F. J., Treister, E., Maccarone, T. J., Coppi, P. S., Maza, J., Zepf, S. E., & Guzman, R. 2003, *AJ*, 125, 1689  
 Cavaliere, A., & Vittorini, V. 2000, *ApJ*, 543, 599  
 Cowie, L. L., Barger, A. J., Bautz, M. W., Brandt, W. N., & Garmire, G. P. 2003, *ApJ*, 584, L57  
 Croom, S. M., Smith, R. J., Boyle, B. J., Shanks, T., Miller, L., Outram, P. J., & Loaring, N. S. 2004, *MNRAS*, 349, 1397  
 Dickey, J. M., & Lockman, F. J. 1990, *ARA&A*, 28, 215  
 Fabian, A. C. 1999, *MNRAS*, 308, 39  
 Fan, X., et al. 2001, *AJ*, 121, 54  
 ———. 2004, *AJ*, 128, 515  
 Fiore, F., et al. 2003, *A&A*, 409, 79  
 Francis, P. J., Nelson, B. O., & Cutri, R. M. 2004, *AJ*, 127, 646  
 Fukugita, M., Ichikawa, T., Gunn, J. E., Doi, M., Shimasaku, K., & Schneider, D. P. 1996, *AJ*, 111, 1748  
 Giacomini, R., et al. 2002, *ApJS*, 139, 369

- Gilli, R., Salvati, & M., Hasinger, G. 2001, *A&A*, 366, 407  
Gilli, R., et al. 2003, *ApJ*, 592, 721  
Green, P. J., et al. 2004, *ApJS*, 150, 43  
Hasinger, G., Miyaji, T., & Schmidt, M. 2005, *A&A*, submitted  
Hasinger, G., et al. 2001, *A&A*, 365, L45  
Kauffmann, G., & Haehnelt, M. 2000, *MNRAS*, 311, 576  
Kim, D.-W., et al. 2004a, *ApJ*, 600, 59  
———. 2004b, *ApJS*, 150, 19  
Lehmann, I., et al. 2001, *A&A*, 371, 833  
Menci, N., Fiore, F., Perola, G. C., & Cavaliere, A. 2004, *ApJ*, 606, 58  
Miyaji, T., Hasinger, G., & Schmidt, M. 2000, *A&A*, 353, 25  
———. 2001, *A&A*, 369, 49  
Page, M. J., Carrera, F. J. 2000, *MNRAS*, 311, 433  
Rosati, P., et al. 2002, *ApJ*, 566, 667  
Sanders, J. S., & Fabian, A. C. 2001, *MNRAS*, 325, 178  
Schmidt, M. 1968, *ApJ*, 151, 393  
Schmidt, M., Schneider, D. P., & Gunn, J. E. 1995, *AJ*, 110, 68  
Schwope, A., et al. 2000, *Astron. Nachr.*, 321, 1  
Silverman, J. D., et al. 2002, *ApJ*, 569, L1  
———. 2005, *ApJ*, 618, 123  
Steffan, A. T., Barger, A. J., Cowie, L. L., Mushotzky, R. F., & Yang, Y. 2003, *ApJ*, 596, L23  
Szokoly, G. P., et al. 2004, *ApJS*, 155, 271  
Treister, E., Castander, F. J., Maccarone, T. J., Herrera, D., Gawiser, E., Maza, J., & Coppi, P. S. 2004, *ApJ*, 603, 36  
Ueda, Y., Akiyama, M., Ohta, K., & Takamitsu, M. 2003, *ApJ*, 598, 886  
Warren, S. J., Hewett, P. C., & Osmer, P. S. 1994, *ApJ*, 421, 412  
Wilkes, B. J., Schmidt, G. D., Cutri, R. M., Ghosh, H., Hines, D. C., Nelson, B., & Smith, P. S. 2002, *ApJ*, 564, L65  
Wolf, C., Wisotzki, L., Borch, A., Dye, S., Kleinheinrich, M., & Meisenheimer, K. 2003, *A&A*, 408, 499